Journal of Materials Chemistry A

PAPER

View Article Online
View Journal | View Issue

Cite this: J. Mater. Chem. A, 2014, 2, 11171

Thermoelectric properties of p-type polycrystalline SnSe doped with Ag†

Cheng-Lung Chen,‡[ab] Heng Wang,‡[a] Yang-Yuan Chen,[b] Tristan Day[a] and G. Jeffrey Snyder*[a]

Received 4th April 2014
Accepted 2nd May 2014

DOI: 10.1039/c4ta01643b

www.rsc.org/MaterialsA

Many IV–VI semiconductors tend to be good thermoelectric materials, these include all Pb chalcogenides as well as Pb-free SnTe: all of which crystallize in a NaCl cubic structure. Another group of IV–VI compounds form layered orthorhombic structures. SnSe is one of these compounds, whose transport properties as a polycrystalline thermoelectric material have rarely been studied. Here we present our study of p-type polycrystalline SnSe doped with Ag, prepared by melting and hot pressing. SnSe has anisotropic properties with hysteresis observed in resistivity between 300 and 650 K regardless of doping. Ag is not an ideal dopant but is able to increase the carrier density significantly, as a result a peak zT of 0.6 was observed at 750 K. Transport properties of doped SnSe can be explained with a single parabolic band model, which suggests promising potential for this compound together with its challenges.

1. Introduction

Thermoelectric materials are semiconductors that enable direct conversion between heat and electricity. Devices using these materials are being used in solid state cooling as well as power supplies.[1] The performance of materials as thermoelectrics can be evaluated with the dimensionless figure of merit, $zT = \sigma S^2 T/\kappa$, where S, T, σ and κ are the Seebeck coefficient, absolute temperature, electrical and thermal conductivity, respectively. At around 500 °C the highest zTs are seen in IV–VI compounds such as PbTe,[2,3] PbSe[4,5] and PbS.[6] In spite of the continuous progress in advancing the performance of these materials,[7–12] the presence of Pb has limited their future in domestic applications. SnTe could be an alternative according to a recent study[13] but the use of Te is still a big disadvantage for domestic devices that are more cost-sensitive. The other IV–VI compounds, including SnSe, have not been studied as carefully in polycrystalline form,[14] compared with the compounds mentioned above. High thermoelectric performance has just recently been reported[15] in undoped, single crystal SnSe accelerating interest in this material.

Unlike its heavier analogs with a NaCl type structure, SnSe crystallizes in a layered structure with zigzagged atomic chains with orthorhombic symmetry below 810 K.[16,17] It undergoes a phase transition above that temperature, which alters the zigzag chains so that the atoms are stacked with a configuration that resembles the rock-salt but with stacking faults every other (001) plane.[18] This leads to a considerable difference in the band structure and transport properties between this compound and the rock-salt IV–VI compounds.

In this paper we discuss the synthesis and transport properties of p-type polycrystalline SnSe as a potential thermoelectric material. Stoichiometric SnSe is found to be a semiconductor with very low intrinsic defect concentration and high resistivity. Extra free carriers, in this case holes, can be introduced by substituting Sn with Ag. For the sample $Ag_{0.01}Sn_{0.99}Se$, zT is found to be 0.6 at 750 K, higher than that of an undoped SnSe (0.3) due to an increase of the charge carrier density. SnSe could be a promising thermoelectric material, given some challenges could be resolved.

2. Experimental

Elements Ag, Sn, and Se, all of purity of 99.999% were loaded into quartz ampoules. The ampoules were then evacuated, sealed, and slowly heated up to 1200 K, and kept for 12 hours followed by water quenching. The obtained ingots were further annealed at 800 K for 72 hours. The annealed ingots were ground to powders with an agate mortar, and then hot pressed using an induction heating rapid hot press[19] at 800 K, 36 MPa under 1 atm argon for 10 minutes to form a dense pellet 12 mm in diameter. Two sheets of samples were cut along different directions for measurement, with the relative density being not less than 96% of the theoretical value (6.18 g cm^{-3}). The grain size is estimated to be between 10 and 100 μm, which according to our previous experience on lead chalcogenides,[6] leads to negligible influence on electron and phonon transport. The

[a]Materials Science, California Institute of Technology, Pasadena, CA 91125, USA. E-mail: jsnyder@caltech.edu

[b]Institute of Physics, Academia Sinica, Taipei 11529, Taiwan

† Electronic supplementary information (ESI) available: Heat capacity, transport property measurements along two different directions for all samples, and additional transport properties. See DOI: 10.1039/c4ta01643b

‡ These authors contributed equally to this work.

phase composition is analyzed by powder X-ray diffraction (XRD), performed with a diffractometer (PANalytical X'Pert Pro) equipped with Cu Kα radiation. The microstructures of samples are investigated using a scanning electron microscope (SEM, ZEISS). The compositions of the phase and the distributions of elements are determined using a X-ray energy dispersive spectrometer (EDS, Oxford Instrument X-Max). Two-dimensional Seebeck coefficient maps and their corresponding histograms are determined from a scanning Seebeck coefficient measurement system[20] developed at the California Institute of Technology. The temperature dependent Seebeck coefficient is determined by measuring the voltage difference on two sides of the sample using chromel–niobium thermocouples under an oscillating temperature gradient of 0 to 15 K with constant ambient temperature.[21] Electrical resistivity and Hall effect are measured using the Van der Pauw method in a magnetic field up to $\pm 2T$.[22] The thermal conductivity is calculated from $\kappa = \rho C_p D_T$. The thermal diffusivity, D_T, is measured by a laser flash method (Netzsch LFA 457) under Ar flow using Cowan model plus pulse correction. The heat capacity values C_p are obtained using a suggested fitting equation given by Pashinkin *et al.* based on experimental results,[23] which is consistent with experimental values reported for higher temperatures[24] from Yamaguchi *et al.* (plot of C_p shown in the ESI†). Density ρ is calculated using the measured dimensions and weight. During all measurements data are acquired during both heating and cooling. The uncertainty of each measurement is estimated to be approximately 5%, which leads the combined experimental uncertainty of zT to be about ~20%.

3. Results and discussion

3.1 Synthesis and characterization

X-ray diffraction data of samples with the nominal Ag compositions staring from 0 to 7% are shown in Fig. 1a. The patterns can be indexed to the low temperature SnSe phase (JCPDS #140159) with an orthorhombic structure. A small amount of secondary phase, denoted by arrows, is seen in Ag doped samples and is identified to be the $AgSnSe_2$ phase (JCPDS #331194) with cubic structure. The existence of $AgSnSe_2$ is also confirmed by the back-scattered electron (BSE) images of polished surfaces of all Ag doped samples. The SEM micrograph and EDS mapping image of the 1% Ag sample are shown in Fig. 1b as an example. Ag segregates in regions of few microns even for as little as 1% Ag addition. Scanning Seebeck coefficient mapping on $Ag_{0.01}Sn_{0.99}Se$ and $Ag_{0.05}Sn_{0.95}Se$ (Fig. 1c and d) revealed small regions with abnormally low Seebeck coefficients that likely originate from the metallic secondary phase. As with SEM the Seebeck mapping shows that all these regions are isolated without forming a linked network. Using an effective medium model[25,26] we estimated the effect of the secondary $AgSnSe_2$ phase on the electrical conductivity and Hall coefficient to be less than 10%.

Stoichiometric SnSe shows p-type intrinsic behavior with low carrier density on the order of low 10^{17} cm^{-3}. With up to 5% of extra Se the compound shows largely the same transport behavior with negligible carrier density change; whereas with

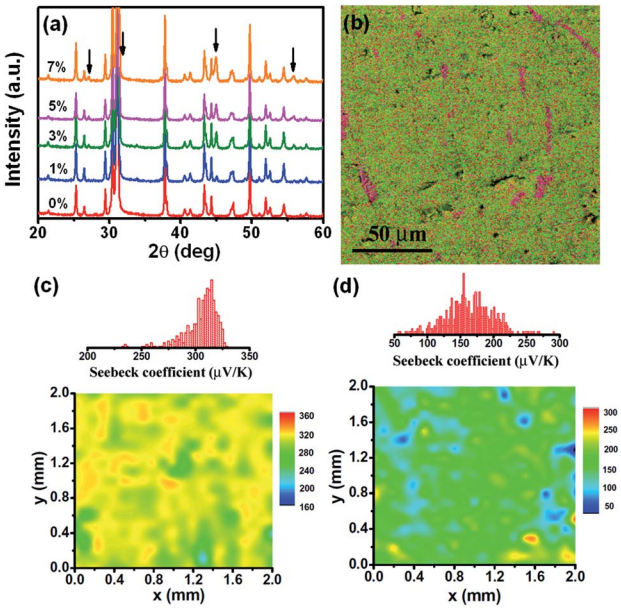

Fig. 1 (a) XRD patterns of SnSe alloying with different Ag concentrations indicate SnSe and a small amount of $AgSnSe_2$ phase (arrows). (b) EDS mapping images of 1% Ag alloyed SnSe alloys. The Ag area is marked pink. (c) and (d) Scanning Seebeck coefficient measurement results and histograms of 1% and 5% Ag-alloyed SnSe alloys, respectively.

5% extra Sn the compound becomes slightly n-type (but not stable) (Fig. 2a and b). Unlike Pb chalcogenides, SnSe is fairly difficult to dope.[27–30] Various candidates as dopants were attempted (Br, Sb, Bi and In as donors; Na, Ag, and Tl as acceptors), but only Na and Ag seem to be able to increase the carrier density to the concentrations usually required for good thermoelectric performance. While Na provides better efficiency and higher carrier density, samples doped with Na are not stable upon repeated heating and cooling. As a result, Ag is used as the dopant for this study. As shown in Fig. 2c, with

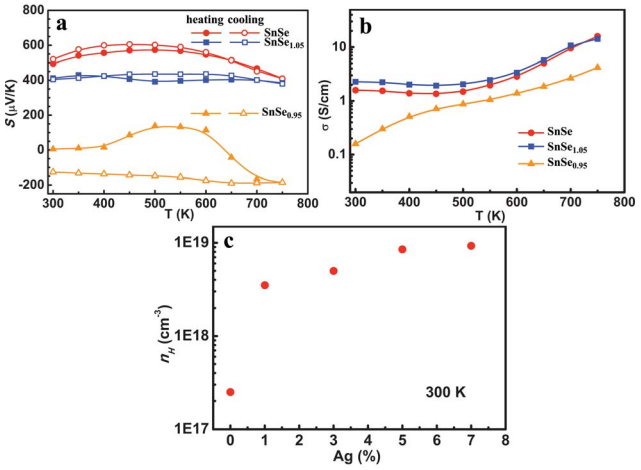

Fig. 2 Seebeck coefficients (a) and electrical conductivity (b) as a function of temperature for Sn_1Se_1, $Sn_1Se_{1.05}$, and $Sn_1Se_{0.95}$. (c) Measured Hall carrier concentration as a function of Ag content at 300 K.

addition of Ag, the carrier density can be gradually increased and saturated at about 9×10^{18} cm^{-3} for the $Ag_{0.07}Sn_{0.93}Se$ sample. The doping efficiency is poor on the order of 1%, which is consistent with microstructural observation. The solubility of Ag in SnSe is very small but seems to be sensitive to the actual composition so that the systematic change of the Ag content has resulted in a very slight change of Ag solubility, which is reflected in the increase of carrier density.

3.2 Electrical and thermal transport properties

All SnSe samples show hysteresis during heating and cooling (more in resistivity and less in Seebeck coefficient) between 300 to 650 K. Altering the Sn : Se ratio, as well as doping with Ag fails to eliminate the hysteresis. The Differential Scanning Calorimetry (DSC) showed very small peaks around 430 K, 580 K and 610 K, respectively (see ESI†). The phase transition in SnSe was reported to occur at 809 K,[18] other processes, are thus responsible for hysteresis in resistivity as well as the peaks seen in DSC. Despite the hysteresis, the transport properties of the Ag doped samples are consistent upon several repeated heating and cooling measurements (Fig. 3), suggesting that the hysteresis in these samples is more likely caused by reversible processes rather than non-equilibrium states of the samples. For clarity in the following discussions only results measured during cooling are shown, the heating process reveals the same trend only with different absolute values (Fig. S1†).

Fig. 4 shows the temperature dependence of transport properties for samples with different Ag contents. These are the properties measured along the direction perpendicular to the hot press direction. The resistivity at room temperature dropped significantly with Ag doping, yet at 750 K the resistivities of doped samples are still several times higher than typical good thermoelectrics. The resistivity is anisotropic and the in-plane result (perpendicular to the hot press direction) is about 40% lower than the other direction (Fig. 5 and S2 to S4†).

The temperature dependent Seebeck coefficients are shown in Fig. 4b. High S values are seen for all samples, even the one with the largest carrier density 9×10^{18} cm^{-3} shows S around 200 μV K^{-1} at room temperature. A maximum is seen in the results for SnSe and $Ag_{0.01}Sn_{0.99}Se$, the other two samples with higher Ag content have very weak temperature dependence. A maximum in the Seebeck coefficient is usually a result of bipolar conduction (noticeable minority carriers being excited) where from the peak value a band gap of about 0.5 eV can be

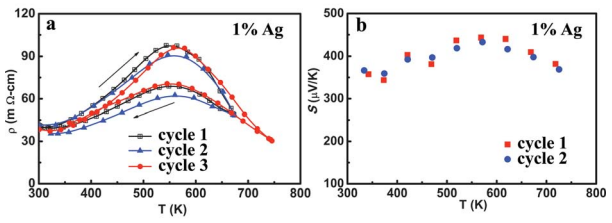

Fig. 3 Temperature dependent resistivity (a) and Seebeck coefficients (b) of 1% Ag alloyed SnSe after several repeated heating and cooling tests.

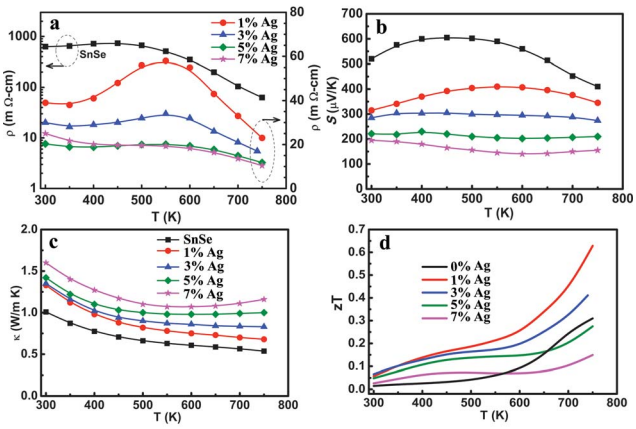

Fig. 4 Temperature dependence of electrical resistivity (a), Seebeck coefficients (b), thermal conductivity (c) and zT (d) for Ag-alloyed SnSe.

estimated,[31] roughly consistent with the recently reported[15] band gap of 0.8 eV. Bipolar conduction could contribute here, although there are also indications that point to other possibilities as discussed later.

For all samples the Hall mobility decreases with temperature roughly following a $T^{-1.5}$ relationship, shown in Fig. 6 (data shown are smoothed fitting result, raw data showed considerable scattering due to large contact resistance in Van de Pauw measurement (Fig. S5†)). This enables us to use the simple single parabolic band model with acoustic phonon scattering approximation to understand the change of transport properties with doping. At 300 K, the change of the Seebeck coefficient with carrier density (Pisarenko relation) has suggested a density of state effective mass m_d^* of $0.75m_e$ (Fig. 7a), where m_d^* was

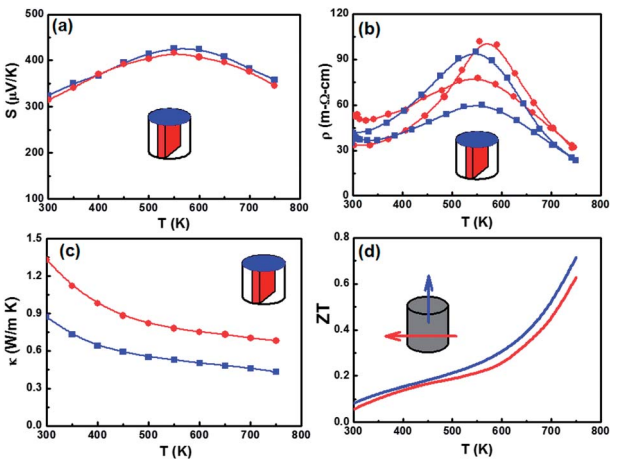

Fig. 5 (a) Seebeck coefficients, (b) electrical resistivity, (c) thermal conductivity, and (d) zT of two slices cut from a single cylinder (1% Ag) along different directions. Different colours in (a–c) represent results measured from each slice of the cylinder, while the colours in (d) represent zT calculated from properties measured along each direction.

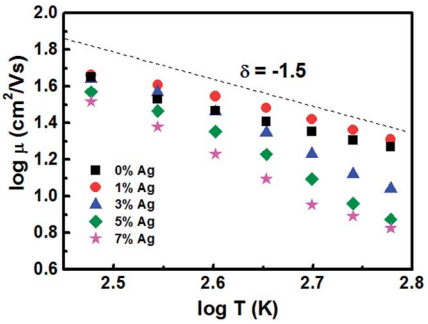

Fig. 6 log μ–log T plots of SnSe alloys indicating the linear regime with a slope of $\delta = -1.5$.

determined by the Hall carrier density ($n_H = n/r_H$, assuming spherical Fermi surface) *via*:

$$n = \frac{(2m_d^* k_B T)^{3/2}}{2\pi^2\hbar^3} F_{1/2}(\eta) \quad (1)$$

$$r_H = \frac{3}{4}\frac{F_{1/2}(\eta)F_{-1/2}(\eta)}{F_0(\eta)^2} \quad (2)$$

using the reduced chemical potential η from the Seebeck coefficient:

$$S = \frac{k_B}{e}\left(\left[\frac{2F_1(\eta)}{F_0(\eta)} - \eta\right]\right) \quad (3)$$

$F_x(\eta)$ are the Fermi integrals:

$$F_x(\eta) = \int_0^\infty \frac{\varepsilon^x}{1+\exp(\varepsilon-\eta)}d\varepsilon \quad (4)$$

The drift mobility governed by the acoustic phonon scattering process depends on the chemical potential *via*:

$$\mu = \mu_0\frac{\sqrt{\pi}}{2}\frac{F_0(\eta)}{F_{1/2}(\eta)} = \frac{2^{1/2}\pi\hbar^4 e C_l N_V^{5/3}}{3m_d^{*5/2}(k_B T)^{3/2}\Xi^2}\frac{F_0(\eta)}{F_{1/2}(\eta)} \quad (5)$$

C_l is the average longitudinal elastic constant, N_v is the valley degeneracy of the band, and Ξ is the deformation potential coefficient. Measured Hall mobility ($\mu_H = \mu r_H$) *versus* Hall carrier density can be well explained with this equation (Fig. 7b). The parameter μ_0 stands for the mobility extrapolated to the nondegenerate limit, and is found to be 41 $cm^2 V^{-1} s^{-1}$ by fitting experimental results. Band structure calculation[32] has suggested that the maximum of the valence band in SnSe is on the Λ symmetry line between gamma and Z, having a valley degeneracy of 2. Assuming C_l of SnSe to be the same as that of SnTe (58 GPa) the deformation potential coefficient is estimated to be 24 eV, being comparable to those found in rock-salt Pb chalcogenides.[6]

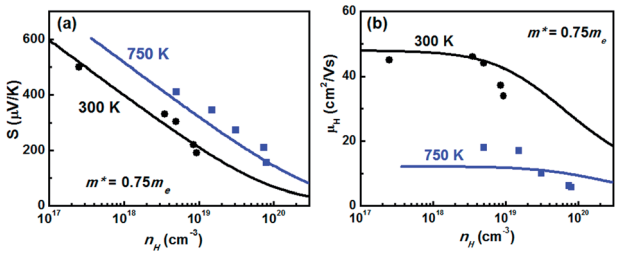

Fig. 7 Seebeck coefficient (a) and Hall mobility (b) as a function of Hall carrier density at 300 and 750 K, respectively.

Using the same parameters determined at 300 K, the SPB model further explained the Pisarenko relation at 750 K (Fig. 7). Usually with bipolar conduction, the measured Seebeck coefficient should be lower than the modeling result using SPB. This being not the case for Ag doped SnSe implies that there may be other possible reasons for the decrease of Seebeck coefficients and increase of carrier density with increasing temperature, such as the temperature dependent defect level or Ag solubility. Similarly the observed mobility values are also comparable with the SPB modeling result: no reduction due to bipolar conduction is seen.

The thermal conductivities κ measured up to 750 K are presented in Fig. 4c. Due to high resistivity the electronic contribution for all samples are negligible. The measurement generally reflects the change of lattice thermal conductivity with temperature. For undoped SnSe the κ_L is found to be 1.1 W m^{-1} K^{-1} at 300 K and decreases with temperature to 0.55 W m^{-1} K^{-1} at 750 K, We notice that this result is lower than historical results on single crystals[33,34] (1.8 W m^{-1} K^{-1} along cleavage plane), as would be expected from the polycrystalline nature of the sample, while the recent study[15] on single crystal SnSe has reported even lower κ_L. Compared to other IV–VI compounds SnSe has a very low lattice thermal conductivity at room temperature, probably due to its complex atomic arrangement relative to the highly symmetric NaCl structure. However, the T^{-1} dependence, a result of the Umklapp process dominated phonon transport, which was seen in rock-salt Pb chalcogenides, is not observed here. The κ_L decreases slowly before saturating at 0.55 W m^{-1} K^{-1}, suggesting a large residual thermal conductivity from the optical phonon contribution.[35] In contrast, κ_L for PbSe at 750 K is about 0.7 W m^{-1} K^{-1}, only slightly larger than SnSe whereas the electrical properties of PbSe are much better. Similar to that found in the resistivity, anisotropy is also seen in the thermal conductivity measured along different directions and the in-plane thermal conductivity is about 60% higher than those along the other direction (Fig. 5c and S4†). Thermal conductivities increase with the increase of Ag contents. This is partly due to the averaging with a metallic secondary phase, which has high thermal conductivity. The higher thermal conductivity could also be related to the possible change in the degree of texturing due to the uniaxial pressure and the presence of ductile metallic $AgSnSe_2$ with low melting temperature.

3.3 Figure of merit

The zT values (in-plane direction) as a function of temperature are calculated using data acquired during the cooling process and the result is shown in Fig. 4d. The zT of the 1% Ag sample

reaches a maximum of ~0.6 at 750 K as compared to 0.3 for the stoichiometric SnSe. Continuous increase in the Ag content and carrier density does not further increase zT. This is because of first the higher thermal conductivity due to increased volume fraction of the secondary phase, and second the lower mobilities. Using the SPB model with parameters determined above ($m_d^* = 0.75m_e$, $N_v = 2$, $C_l = 58$ GPa, $\Xi = 24$ eV, and using $\kappa_L = 0.5$ W m^{-1} K^{-1}), the modeled zT *versus* carrier density at 750 K is plotted in Fig. 8, which predicts a maximum of 0.4 when the carrier density is around 4 to 5 × 10^{19} cm^{-3}. The calculated zT of 0.6 for $Ag_{0.01}Sn_{0.99}Se$ is higher than the predicted maximum, mainly due to the observed mobility being much higher than the model as well as other samples.

The predicted zT for SnSe is somewhat disappointing. There are however two factors not accounted for in the current analysis that could potentially justify higher expectation on zT values. First, the mobility of these samples may be not as high as the cleanest samples, especially when the secondary phase has been found. Assuming the mobility of "clean" samples to be twice as high, the maximum zT would be 0.7 (dashed line in Fig. 8), which is a good start for a Pb-free and Te-free thermoelectric material. Second, unlike the isotropic Pb-chalcogenides, the modeling of transport properties on polycrystalline SnSe in this study is subject to the degree of texturing: theoretically maximum zT can be only achieved when single crystal SnSe is grown and measured along the preferred direction. We notice that independent studies[36–38] have reported for single crystal SnSe a Hall mobility of ~120 cm^2 V^{-1} s^{-1} perpendicular to the c-axis (denoted a-axis in ref. 15), a three-fold difference compared with the highest mobility found in this study, while only a quarter[36] to a half[38] of this along the c-axis. Thus there could be up to a three-fold increase of zT (to 1.2) if single crystals of these samples were grown and tested perpendicular to the c-axis. Nevertheless, further material engineering is needed before p-type SnSe could compete, in terms of average zT, with the best available PbTe or PbSe thermoelectrics. At the same time, the hysteresis issue in properties seen here between 300 and 650 K has to be resolved. Until then, any practical value of SnSe as a thermoelectric material will remain an open question regardless of its peak zT.

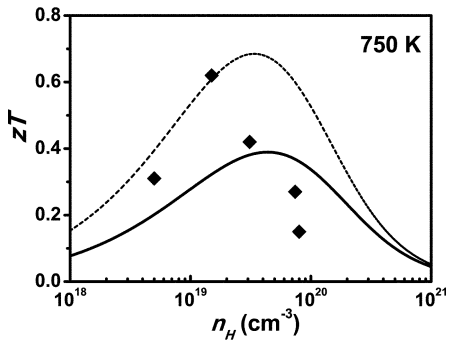

Fig. 8 zT as a function of carrier density at 750 K. The experimental results (symbol) can be predicted by the modeled zT (solid and dashed curves).

4. Conclusions

In summary, polycrystalline SnSe doped with Ag were prepared by melting followed by rapid hot pressing. Undoped SnSe has low carrier density. Doping with Ag increases this to 9 × 10^{18} cm^{-3}. The transport properties, especially resistivity and thermal conductivity are anisotropic. Hysteresis is seen in resistivity between heating and cooling regardless of doping. Transport properties at 300 K and 750 K can be explained with a single parabolic band model and acoustic phonon scattering approximation. The density-of-state effective mass is found to be $0.75m_e$ and the nondegenerate limit drift mobility is 41 cm^2 V^{-1} s^{-1}, both independent of temperature. The peak zT measured at 750 K is 0.6. Although higher zT in doped p-type SnSe is still possible, material engineering is needed for SnSe to be a truly promising thermoelectric material.

Acknowledgements

H. W., T. D. and G. J. S. thank the Bosch-BERN and AFOSR-MURI programs for funding.

References

1 L. E. Bell, *Science*, 2008, **321**, 1457–1461.
2 Y. Pei, A. LaLonde, S. Iwanaga and G. J. Snyder, *Energy Environ. Sci.*, 2011, **4**, 2085–2089.
3 A. D. LaLonde, Y. Pei and G. J. Snyder, *Energy Environ. Sci.*, 2011, **4**, 2090–2096.
4 H. Wang, Y. Pei, A. D. Lalonde and G. J. Snyder, *Adv. Mater.*, 2011, **23**, 1366–1370.
5 H. Wang, Y. Pei, A. D. LaLonde and G. J. Snyder, *Proc. Natl. Acad. Sci. U. S. A.*, 2012, **109**, 9705–9709.
6 H. Wang, E. Schechtel, Y. Pei and G. J. Snyder, *Adv. Energy Mater.*, 2013, **3**, 488–495.
7 Y. Pei, X. Shi, A. LaLonde, H. Wang, L. Chen and G. J. Snyder, *Nature*, 2011, **473**, 66–69.
8 K. Biswas, J. He, I. D. Blum, C. I. Wu, T. P. Hogan, D. N. Seidman, V. P. Dravid and M. G. Kanatzidis, *Nature*, 2012, **489**, 414–418.
9 H. Wang, Z. M. Gibbs, Y. Takagiwa and G. J. Snyder, *Energy Environ. Sci.*, 2014, **7**, 804.
10 L. D. Zhao, S. Hao, S. H. Lo, C. I. Wu, X. Zhou, Y. Lee, H. Li, K. Biswas, T. P. Hogan, C. Uher, C. Wolverton, V. P. Dravid and M. G. Kanatzidis, *J. Am. Chem. Soc.*, 2013, **135**, 7364–7370.
11 L. D. Zhao, J. He, C. I. Wu, T. P. Hogan, X. Zhou, C. Uher, V. P. Dravid and M. G. Kanatzidis, *J. Am. Chem. Soc.*, 2012, **134**, 7902–7912.
12 L. D. Zhao, S. H. Lo, J. He, H. Li, K. Biswas, J. Androulakis, C. I. Wu, T. P. Hogan, D. Y. Chung, V. P. Dravid and M. G. Kanatzidis, *J. Am. Chem. Soc.*, 2011, **133**, 20476–20487.
13 Q. Zhang, B. Liao, Y. Lan, K. Lukas, W. Liu, K. Esfarjani, C. Opeil, D. Broido, G. Chen and Z. Ren, *Proc. Natl. Acad. Sci. U. S. A.*, 2013, **110**, 13261–13266.
14 S. Chen, K. Cai and W. Zhao, *Phys. B (Amsterdam, Neth.)*, 2012, **407**, 4154–4159.

15 L. D. Zhao, S. H. Lo, Y. Zhang, H. Sun, G. Tan, C. Uher, C. Wolverton, V. P. Dravid and M. G. Kanatzidis, *Nature*, 2014, **508**, 373–377.
16 I. Lefebvre, M. A. Szymanski, J. Olivier-Fourcade and J. C. Jumas, *Phys. Rev. B: Solid State*, 1998, **58**, 1896–1906.
17 T. Chattopadhyay, J. Pannetier and H. G. Vonschnering, *J. Phys. Chem. Solids*, 1986, **47**, 879–885.
18 H. Wiedemeier and H. G. von Schnering, *Z. Phys. Chem.*, 1978, **148**, 295–303.
19 A. D. LaLonde, T. Ikeda and G. J. Snyder, *Rev. Sci. Instrum.*, 2011, **82**, 025104.
20 S. Iwanaga and G. J. Snyder, *J. Electron. Mater.*, 2012, **41**, 1667–1674.
21 S. Iwanaga, E. S. Toberer, A. LaLonde and G. J. Snyder, *Rev. Sci. Instrum.*, 2011, **82**, 063905.
22 K. A. Borup, E. S. Toberer, L. D. Zoltan, G. Nakatsukasa, M. Errico, J. P. Fleurial, B. B. Iversen and G. J. Snyder, *Rev. Sci. Instrum.*, 2012, **83**, 123902.
23 A. S. Pashinkin, A. S. Malkova, V. A. Fedorov and M. S. Mikhailova, *Inorg. Mater.*, 2006, **42**, 593–595.
24 K. Yamaguchi, K. Kameda, Y. Takeda and K. Itagaki, *Mater. Trans., JIM*, 1994, **35**, 118–124.
25 D. Stroud, *Phys. Rev. B: Solid State*, 1975, **12**, 3368–3373.
26 V. Guttal and D. Stroud, *Phys. Rev. B: Condens. Matter Mater. Phys.*, 2006, **73**, 085202.
27 J. Umeda, *J. Phys. Soc. Jpn.*, 1961, **16**, 124.
28 B. L. Evans and R. A. Hazelwoo, *J. Phys. D: Appl. Phys.*, 1969, **2**, 1507–1516.
29 A. Agarwal, P. D. Patel and D. Lakshminarayana, *J. Cryst. Growth*, 1994, **142**, 344–348.
30 A. Agarwal, M. N. Vashi, D. Lakshminarayana and N. M. Batra, *J. Mater. Sci.: Mater. Electron.*, 2000, **11**, 67–71.
31 H. J. Goldsmid and J. W. Sharp, *J. Electron. Mater.*, 1999, **28**, 869–872.
32 R. Car, G. Ciucci and L. Quartapelle, *Phys. Status Solidi B*, 1978, **86**, 471–478.
33 J. D. Wasscher, W. Albers and C. Haas, *Solid-State Electron.*, 1963, **6**, 261–264.
34 D. P. Spitzer, *J. Phys. Chem. Solids*, 1970, **31**, 19–40.
35 E. S. Toberer, A. Zevalkink and G. J. Snyder, *J. Mater. Chem.*, 2011, **21**, 15843–15852.
36 S. Asanabe, *J. Phys. Soc. Jpn.*, 1959, **14**, 281.
37 W. Albers, C. Haas, H. Ober, G. R. Schodder and J. D. Wasscher, *J. Phys. Chem. Solids*, 1962, **23**, 215–220.
38 T. H. Patel, R. Vaidya and S. G. Patel, *Bull. Mat. Sci.*, 2003, **26**, 569–574.